Influence of the nanocrystallinity on exchange bias in Co/CoO core/shell nanoparticles

Mario Ávila-Gutiérrez, Arthur Moisset, Anh-Tu Ngo, Salvatore Costanzo, Guilhem Simon, Philippe Colomban, Marc Petit, Christophe Petit, Isabelle Lisiecki

Influence of the nanocrystallinity on exchange bias in Co/CoO core/shell nanoparticles

Mario Ávila-Gutiérrez[1], Arthur Moisset[1], Anh-Tu Ngo[1], Salvatore Costanzo[1], Guilhem Simon[1], Philippe Colomban[1], Marc Petit[2], Christophe Petit[1*], Isabelle Lisiecki[1*]

1-Sorbonne Université, CNRS, MONARIS, UMR8233, F-75005 Paris, France

2-Sorbonne Université, CNRS, Institut Parisien de Chimie Moléculaire, UMR 8232, F-75005 Paris, France

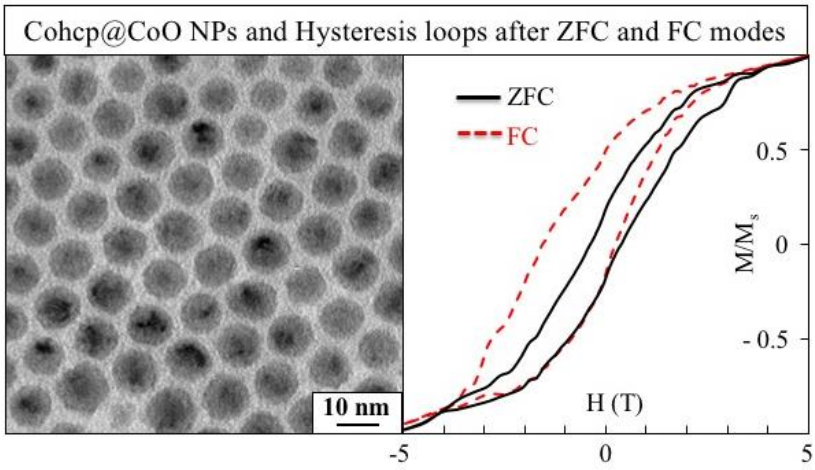

Abstract

This study presents a comparison of the magnetic properties of core/shell nanoparticles composed of cobalt (Co) and cobalt oxide (CoO), with variations in their crystalline structure. Specifically, we investigated poorly crystallized core/shell nanoparticles (with a diameter of 8.8 nm) prepared from face-centered cubic (fcc) cobalt polycrystals synthesized via the micellar approach, as well as highly crystallized nanoparticles (with a diameter of 9.9 nm) prepared from hexagonal (hcp) cobalt single-crystals formed using the organometallic decomposition approach. The oxidation process is conducted in a solution.

To examine the structural characteristics, high-resolution transmission electron microscopy (HRTEM) was employed. Our findings revealed that the Co fcc polycrystals yield a poorly fcc

crystallized CoO shell, whereas the Co hcp nanoparticles exhibited a highly crystallized CoO shell.

Furthermore, we conducted a magnetic investigation utilizing a Vibrating Sample Magnetometer (VSM). The results clearly demonstrate the significant influence of the core/shell nanoparticle's crystalline structure on the interfacial magnetic coupling. Specifically, we observed an exchange bias exclusively in the Co_{hcp}/CoO nanoparticles. Notably, the measured exchange bias field (655 mT) surpasses previously reported values in literature for similar nanoparticles with an hcp cobalt core. This enhancement can be attributed to several factors, including the high-quality Co/CoO interface, the disparate magnetic anisotropy between the core (Co hcp) and the shell (CoO), as well as the optimal ratio between the core and shell, thereby inducing a heightened interfacial magnetic coupling.

1. Introduction

The exchange bias (EB) effect was discovered in 1956 by Meiklejohn and Bean for Co@CoO NPs [1]. It resulted from interfacial exchange coupling between two materials (characterized by a notable difference in magnetic anisotropy), usually, one is ferromagnetic (FM) while the other is antiferromagnetic (AFM). This effect is highlighted by a horizontal shift of the hysteresis loop as well as an increase in the coercivity [2]. For the applications, controlling the exchange bias is of paramount importance. Hence, since its discovery, it has been widely exploited in different systems including spintronic devices such as spin valves [3], sensors [4] and nanostructured permanent magnets [5]. From a fundamental point of view, despite extensive research on both films [6-10] and nanoparticles (NPs) which can be synthesized through chemical process [11-23] or produced using physical approaches [24-27], the underlying mechanism that governs this intricate phenomenon is still not fully understood. This statement is well supported by an important number of recent papers related to experimental and theoretical EB studies [8,10,15,28,29 for example].

For a given combination of FM and AFM materials, it is now well known that EB effect depends on many structural characteristics [2] including the size and the crystalline structure of the nanomaterials. Thus, the optimization of this effect requires an optimal volume ratio of both FM and AFM materials [16,21,23,24,26], a minimal shell thickness, which has to be above a critical value [8,13,18], as well as a high interfacial quality in terms of crystallinity [14,16,17,19,20]. The morphology is another characteristic which can impact the EB effect [13,17,18,22,27]. Based on current understanding, and despite extensive research efforts aimed

at enhancing the EB effect in NPs, which is crucial for the advancement of EB devices, achieving all the necessary conditions in a specific system remains a formidable challenge.

In this paper, our purpose is to control and optimize the crystalline structure of core (Co)/shell (CoO) NPs from poorly to highly crystallized NPs. This achievement has been made possible through our ability to proficiently master two distinct synthesis processes for Co NPs, resulting in the formation of two distinct crystalline structures of metallic cobalt. By using the strategy of chemical reduction in reverse micelles, we form Co fcc polycrystals while the thermal decomposition approach favored highly-crystallized Co hcp single crystals. The partial oxidation of the two types of Co NPs allowed the formation of core (Co) /shell (CoO) NPs with different crystallinities (the core, the shell and at the interface Co/CoO) while keeping almost similar sizes. An accurate comparative magnetic study performed by vibrating sample magnetometry (VSM) of the two populations of partially oxidized NPs clearly showed a drastic effect of the sample crystallinity on the magnetic properties. Co_{fcc}@CoO NPs did not exhibit any horizontal shift of the hysteresis loop while a large one was observed for Co_{hcp}@CoO NPs. This outcome can be attributed to the excellent quality of the Co/CoO interface, along with the distinct magnetic anisotropy observed between the core (Co hcp) and the shell (CoO) in the latter scenario, in contrast to Co_{fcc}@CoO NPs. As a result, a strong interfacial magnetic coupling was induced. To our knowledge, for NPs synthesized via a colloidal approach, the observed value of EB, which is 655 mT for the core (Co_{hcp})/shell (CoO), surpasses those reported in existing literature.

2. Experimental section

2.1. Chemical

All materials were used as purchased without further purification. Cobalt acetate and ethanol (VWR), isooctane and hexane (Sigma Aldrich), sodium di(ethylhexyl) sulfosuccinate (Na(AOT)) (Fluka), and $NaBH_4$ (Acros Organic, 95%); dodecanoic acid (Acros). The synthesis of cobalt (II) bis(2-ethylhexyl)sulfosuccinate, ($Co(AOT)_2$) has been described previously [30]. $CoCl_2.6H_2O$ (Sigma-aldrich, 98%), PPh_3 (fluorochem, 95%), were commercially bought. Ethanol absolu and diethylether were degassed. THF was distillated under nitrogen then dried over molecular sieves, 4Å (Sigma-aldrich) and finally degassed by Argon.

2.2. Synthesis of dodecanoic acid 7.9 nm-Co fcc nanoparticles

Cobalt fcc NPs stabilized by dodecanoic acid chains were synthesized via chemical reduction in reverse micelles (water in oil droplets) as described in a previous paper [31]. The size

polydispersity was optimized by controlling the reducing agent (sodium borohydride) concentration. The NPs were dispersed in hexane. Their mean diameter and size polydispersity were equal to 7.9 nm and 10%, respectively.

2.3. Synthesis of oleylamine 9.0 nm-Co hcp nanoparticles

Cobalt hcp nanoparticles stabilized by oleylamine were synthesized by disproportionation of $CoCl(PPh_3)_3$ as described in a previous paper [32a]: In a controlled environment within a glove box under a nitrogen atmosphere, a mixture was prepared by combining 10 mL of degassed OAm with $[CoCl(PPh_3)_3]$ in a 25 mL vial. The vial was sealed with a septum, which was punctured by a pipette to allow for overpressure. Subsequently, the solution was subjected to stirring and heating using a 50 mL "drysyn" apparatus filled with sand. The mixture was heated by controlling the increase of the temperature from 20 to 190°C in 1h to obtain the nanospheres. Subsequently, the solution was cooled down to room temperature, and the NPs were washed by adding 20 mL of ethanol and then centrifuged for 5 min at 2500 rpm. The blue supernatant was removed, and the resulting black solid was then dispersed in toluene. Their mean diameter and size polydispersity were equal to 9.0 nm and **9%**, respectively. The synthesis of the organometallic precursor $CoCl(PPh_3)_3$ is described in reference [32b].

2.4. Apparatus

(High-resolution) transmission electron microscopy (HRTEM) was performed using a JEOL JEM 2010 UHR microscope equipped with a LaB6 filament and operating at 200 kV. The images were collected with a 4008 x 2672 pixels CCD camera (Gatan Orius SC1000) coupled with the DIGITAL MICROGRAPH software. The samples are prepared by depositing some drops of the colloidal solution on a Cu grid covered with a carbon thin film.

Magnetic measurements were conducted using a Quantum Design vibrating sample magnometer (VSM). In all magnetic measurements, the applied magnetic field was aligned parallel to the substrate. In the FC (Field Cooled) mode, the magnetization versus field measurements were carried out by cooling the samples from 300 K to 3 K in a magnetic field of 5T. For the ZFC (Zero Field Cooled) mode, the samples were cooled from 300 K to 3 K in the absence of field. Hysteresis curves were taken at 3 K for all the samples. Samples were prepared by depositing some drops on a highly oriented pyrolytic graphite (HOPG) substrate.

The exchange bias field is calculated as $H_{EB}=|H_{c1}-H_{c2}|/2$, where H_{c1} and H_{c2} are the negative and positive coercive fields, respectively.

3. Results and discussion

3.1. Elaboration and comparative structural study of Co_{fcc}@CoO and Co_{hcp}@CoO core shell nanoparticles

Co_{fcc}@CoO and Co_{hcp}@CoO core shell nanoparticles were obtained by oxidizing two types of Co NPs differing by their nanocrystallinity, which was either fcc or hcp. In both cases, the oxidation process is conducted in solution (Fig. 1). Initially, a Co NP colloidal solution is prepared with a concentration of 8.10^{-3} M NPs and transferred to a beaker. The atmosphere of the beaker was then saturated with O_2 for a duration of 5 min, taking care to prevent direct gas injection into the solution. Subsequently, O_2 was allowed to gradually diffuse into the solution. This experimental procedure, which avoids direct bubbling of gas into the NP solution, enabled the gradual diffusion of the gas leading to an optimal control of the partial oxidation of Co nanocrystals resulting in the formation of well-defined core-shell structures.

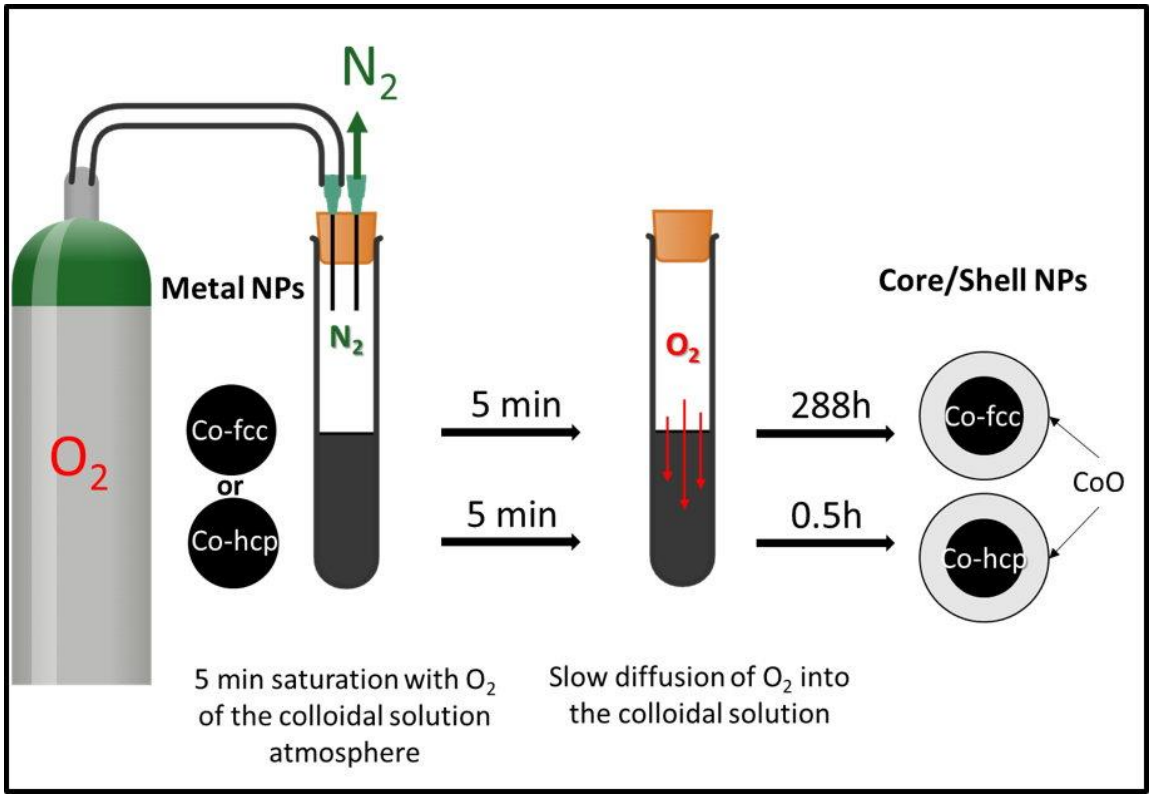

Figure 1. Schematic diagram of the preparation process of Co@CoO core/shell nanoparticles.

3.1.1. Co_{fcc}@CoO core shell nanoparticles

3.1.1.1. Co fcc nanoparticle synthesis

Co fcc NPs used to form Co_{fcc}@CoO core shell NPs, are synthesized by chemical reduction in reverses micelles (Experimental section) [31]. They are characterized by a mean diameter and size polydispersity equal to 7.9 nm and **10%**, respectively (Fig. 2A) and are passivated with dodecanoic acid which gives them a great stability against coalescence and undesirable oxidation [33,34]; the colloidal solvent is hexane. (HR)TEM image of one single particle (Fig. 2C) showed small crystallized domains (less than 1nm) indicating the low crystallinity of the metallic cobalt. This statement is further confirmed through the diffraction pattern (Fig. 2B) which revealed two diffuse rings at 2.00 Å and 1.24 Å, which were indicative of the (111) and (220) lattice spacings of fcc cobalt; no cobalt oxide is detected.

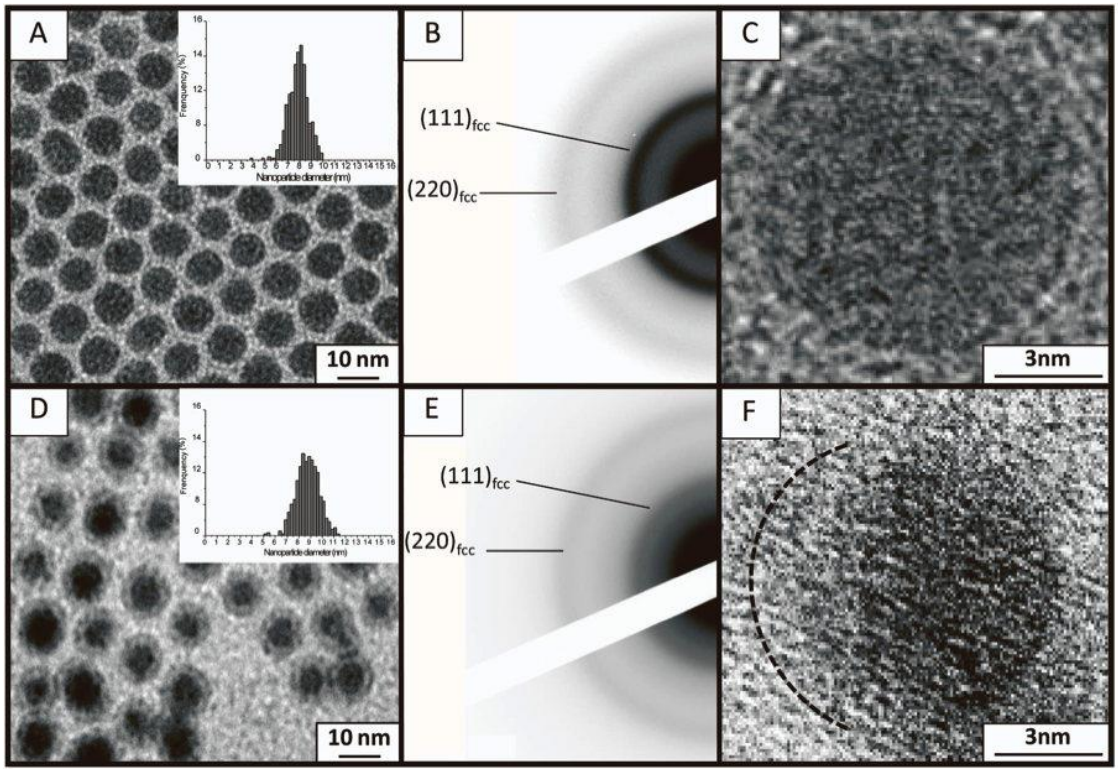

Figure 2. (A) TEM image of 7.9 nm Co fcc nanoparticles, (B) corresponding electron diffraction pattern and (C) HRTEM image of a single nanoparticle. (D) TEM image of 8.8 nm Co_{fcc}@CoO nanoparticles, (E) corresponding electron diffraction pattern and (F) HRTEM image of a single nanoparticle.

3.1.1.2. Core (Co_{fcc})/shell (CoO) nanoparticle formation

Before a 12-day diffusion period with O_2, the (HR)TEM study did not allow the detection of core/shell structures. However, starting from the 12th day, the formation of NPs characterized by a core/shell contrast was observed (Fig. 2D). The mean diameter of the Co core and thickness

of the cobalt oxide shell were determined to be 4.4 nm and 2.2nm, respectively, resulting in a total size of 8.8 nm with a size polydispersity equal to 11%. The absence of crystallinity for the shell (Figs. 2E, F) made it difficult to discriminate between the two possible cobalt oxide, CoO or Co_3O_4. However, considering the formation of the spinel structure Co_3O_4 which typically requires high temperatures [35,36], and the fact that we conducted the experiments at room temperature, we can exclude this possibility. Thus, we concluded that the core (Co_{fcc})/shell (CoO) structure was obtained at room temperature. The slightly larger average diameter (8.8 nm), compared to the 7.9 nm observed for pure Co NPs, can be attributed to the lower density of the CoO material compared to the fcc metallic cobalt. Additionally, we observed that these partially oxidized NPs were highly stable and did not coalesce (Fig. 2D). This feature indicated that dodecanoic acid, similar to pure Co NPs, serves as a ligand in providing stability. The role of the ligand must be emphasized here: as demonstrated by Kazmierczak et al. [37], the carboxylate group interacts by bridging the Co^{2+} ions on the particle surface, which not only effectively protects against coalescence and ensures colloidal stability, but also protects against oxidation, which explains the time required to obtain the oxide shell.

3.1.2. Co_{hcp}@CoO core shell nanoparticles

3.1.2.1. Co hcp nanoparticle synthesis

Co hcp NPs used to form Co_{hcp}@CoO core shell NPs, were synthesized using the organometallic decomposition approach (Experimental section) [32]. Conversely to the Co fcc NPs, they were passivated with oleylamine and dispersed in toluene. Their mean diameter and size polydispersity are equal to 9.0 nm and 9 % respectively (Fig. 3A). The electron diffraction pattern (Fig. 3B), shows 7 sharp rings at 2.13, 1.97, 1.87, 1.52, 1.20, 1.14 and 1.04 Å corresponding to the (100), (002), 101), (102), (110), (103) and (112) of hcp Co. Note that the rings at 1.20 and 1.52 Å could also indicate the presence of the (311) and (220) planes of CoO. However, because we could not observe the other reflections of CoO, we can conclude that pure hcp Co is formed without CoO. The high crystallinity of these Co hcp NPs is clearly illustrated in the high-resolution image of a single particle (Fig. 3C), where regular 2.00 and 2.15 Å spacing can be observed. These are the characteristic distances of the (002) and (100) planes of hcp Co.

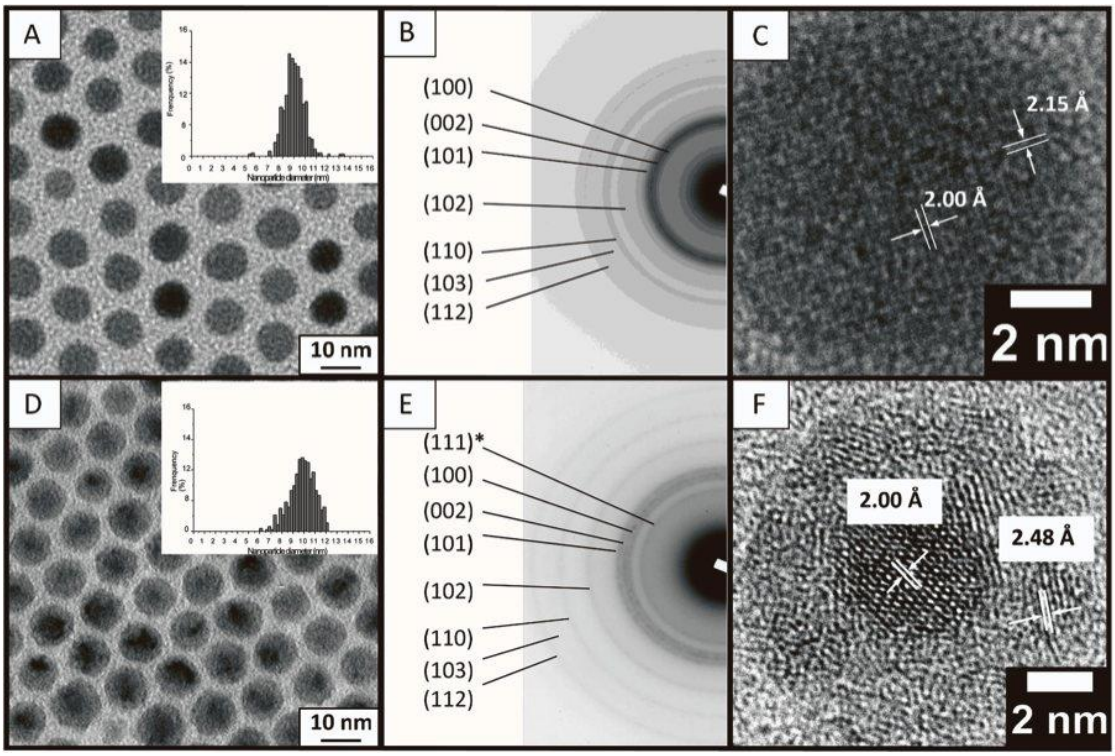

Figure 3. (A) TEM image of 9.0 nm Co hcp nanoparticles, (B) corresponding electron diffraction pattern and (C) HRTEM image of a single nanoparticle. (D) TEM image of **9.9** nm Co_{hcp}@CoO nanoparticles, (E) corresponding electron diffraction pattern and (F) HRTEM image of a single nanoparticle.

3.1.2.2. Core (Co_{hcp})/shell (CoO) nanoparticle formation

The process employed for partially oxidize Co fcc polycrystals was likewise applied to Co hcp single crystals. As a result of this solution oxidation process, which exhibits high reproducibility, pure oleylamine coated Co hcp NPs underwent a transformation into core/shell geometry. It is noteworthy that this transformation occurred at an earlier stage, specifically after a diffusion time of 30 min with O_2, compared to dodecanoic acid coated Co fcc NPs, which took 12 days. This discrepancy is attributed to the stronger interaction between dodecanoic acid ligand/cobalt compared to oleylamine [37]. Indeed, amine adsorption takes place on the surface of the metallic cobalt due to the interaction between the free amine doublet and is thus less effective in protecting against oxidation, as shown by the difference in kinetics with Co fcc. Nevertheless, it is strong enough to prevent the coalescence in solution.

Following a diffusion time of 4 days with O_2, the core@shell NPs possessed a core diameter and a shell thickness of 3.7 nm and 3.1 nm, respectively, which resulted to a total particle size equal to 9.9 nm and a size polydispersity equal to 12 % (Fig. 3D). The corresponding electron

diffraction pattern (Fig. 3E) exhibited distinctive features of both hcp Co and CoO. The observed rings at 2.14, 1.96, 1.89, 1.46, 1.20 and 1.15 Å corresponded to the (100), (002), (101), (102), (110) and (103) and (112) planes of the hcp Co, respectively. Additionally, the presence of CoO is clearly evidenced by the ring at 2.50 Å which corresponds to the (111) planes. Although it is possible that the two rings at 1.20 and 1.46 Å corresponding to the (311) and (220) planes of CoO were present, their close proximity to those of hcp Co, made their distinction difficult. Furthermore, (HR)TEM study revealed the formation of Co hcp single-crystalline cores surrounded by a shell composed of relatively large CoO crystallized domains (~2 nm) with varying orientations (Fig. 3F). The high hcp crystallinity of the Co core was confirmed by the presence of regularly spaced lattice planes with a characteristic distance of 2.00 Å, corresponding to the (002) of hcp Co. The crystallized nanodomains in the shell exhibited one type of regular lattice planes, which were identified as the (111) spacing of CoO, characterized by a distance of 2.50 Å.

This structural study clearly evidenced the formation of Co_{hcp}@CoO NPs characterized by a high crystallinity in both the core and the shell. The epitaxial growth of CoO on the surface of the Co hcp shell is highly probable due to the exceptional crystallinity of the initial hcp Co nanoparticles (NPs) and the employed oxidation technique. This is well supported by different systems featuring highly crystalline Co and CoO nanomaterials, reinforcing the presence of a Co_{hcp}/CoO_{fcc} interface. Notably, Berger et al. [7] convincingly demonstrated a continuous and epitaxial layer of CoO, measuring 2 nm in thickness, on the Co hcp layer. Moreover, Gatel et al. [17] conducted a study revealing another instance of an epitaxial interface in Co_{hcp}/CoO_{fcc} core-shell nanowires where the epitaxy was observed on both the tips and the edges of nanowires. In this case, the CoO shell thickness was 1.2 nm on the edges and 1.4 nm on the tips of the Co cores (12 nm x 130 nm).

As for Co_{fcc}@CoO NPs, Co_{hcp}@CoO NPs were highly stable against coalescence which indicated that oleylamine still played the role of ligands for CoO shell.

The comparative structural study presented here, shows an important effect of the starting Co NP nanocrystallinity on the oxidation process. The same process used to oxidize poorly Co fcc NPs and Co hcp single crystals resulted in amorphous and highly crystallized CoO shells, respectively. This result shows that a high crystallinity of the CoO shell requires a highly-crystallized starting nanomaterial. Moreover, the clear identification of CoO surrounding Co hcp NPs, reinforces our theory that CoO oxide (but amorphous ones) grows at the surface of Co fcc NPs.

3.2. Comparative magnetic study of Co_{fcc}@CoO and Co_{hcp}@CoO core shell nanoparticles

In order to study the effect of the crystallinity of the Co@CoO NPs on the exchange bias effect, a comparative high field study was performed with Co_{fcc}@CoO and Co_{hcp}@CoO NPs.

For both samples, the magnetization versus field measurements were carried out by cooling the sample from 300K to 3K in a magnetic field equal to 5T (*FC mode*). Prior to the field cooling which was performed at above the Néel temperature (T_N) of CoO, 293 K, the spins in the FM (Co core) were aligned parallel to the applied magnetic field while the spins in the AFM (CoO shell) were randomized. Upon field cooling to 3K ($< T_N$), magnetic order was established in the AFM, resulting in an antiparallel configuration of the spins. During the cooling, if the FM and AFM interacted, it signified that the interfacial spins in the Co core and in the CoO shell lay in the same direction. During the magnetization versus field measurements, when the field is inverted (to negative values), the spins in the FM began to flip. However, if the magneto-crystalline anisotropy of the AFM was large enough, their spins remained fixed. The latter tend to retain the spins reversal of the Co FM and the magnetic field required to invert the magnetization in the FM material and as such, was therefore superior compared to that without FM/AFM coupling. Conversely, when the magnetic field returned to positive values, spin reversal in the FM was facilitated, compared to the case without FM/AFM coupling. The consequence was a dissymmetry of the hysteresis curve along the axis of the magnetic field.

For both core/shell samples as well as for the non-oxidized cobalt NPs (fcc and hcp), classical hysteresis, in the zero-filed-cooled mode, were also carried out. The samples were cooled from 300 K to 3 K in the absence of field.

All magnetic hysteresis were carried out with the field applied parallel to the substrate.

As references, the high field behavior of the Co fcc and Co hcp NPs (used for the oxidation step) were also studied. Figures 3A, 4A show the hysteresis in ZFC mode for the 7.9 nm-Co fcc and 9 nm-Co hcp NPs. Figures 3B, 4B show the hysteresis in ZFC and FC modes for the oxidized NPs, i.e., Co_{fcc} (4.4 nm)@CoO (2.2 nm) and Co_{hcp} (3.7 nm)@CoO (3.1 nm).

3.2.1. Co_{fcc} (4.4 nm)@CoO (2.2 nm) core shell nanoparticles

For the starting Cofcc NPs (ZFC mode) (Fig. 4A), the saturation was reached at around 3 T indicating the alignment of all the spins. The value of the coercive field (H_c) was found at 160 mT with a ratio of remanent-to-saturation magnetization (Mr/Ms) of 0.50 (Table 1). These values are in good agreement with those found in the literature for pure metal dodecanoic-coated Co NPs [34]. After the partial oxidation of Co fcc NPs into Co_{fcc}@CoO, we observed a significant increase in H_c from 160 to 185 mT, the other characteristics remained unchanged.

This behavior well accounts for the formation of an AFM shell surrounding the FM core [23, 38] (Table 1). In order to study a possible exchange bias effect in this system, the magnetization curves were performed by cooling the sample under a magnetic field of 5T. The magnetic curve remained similar to that obtained in ZFC mode (Fig. 4B). No shift of the hysteresis curve along the axis of the magnetic field was observed. The coercivity enhancement compared to the Co NPs (*in FC and ZFC modes*) without any loop shift for Co_{fcc}@CoO NPs (*in FC mode*) is explained by the overly small anisotropy of the CoO shell, which is inherent to its amorphous structure. The absence of magnetic order of the spins in the AFM, resulted in an inordinately small FM/AFM coupling and then, in the absence of exchange bias. [2].

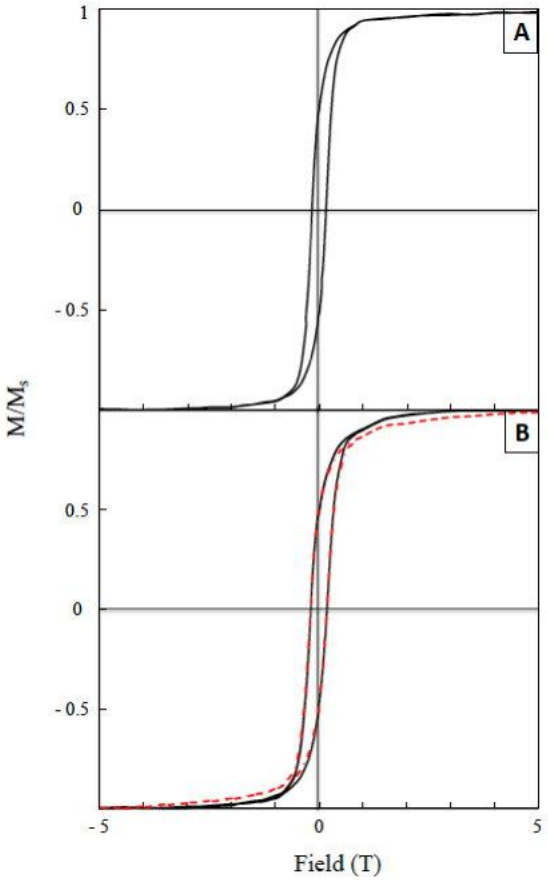

Figure 4. Hysteresis curves taken at 3K of (A) Co fcc nanoparticles (solid line) and (B) Co_{fcc}@CoO nanoparticles in ZFC mode (solid line) and FC mode (dashed line).

Table 1

Structural and magnetic characteristics of Co fcc, Co hcp, Cofcc@CoO and Cohcp@CoO nanoparticles, extracted from TEM and the hysteresis loops of the zero- field cooled (ZFC) and field-cooled (FC) in a magnetic field of 5 T. Mr/Ms: ratio of remanent-to-saturation magnetization, Hc: coercive field.

Structural parameters	Co_{fcc}	Co_{fcc}@CoO	Co_{hcp}	Co_{hcp}@CoO
D_{TEM} (nm)	7.9	8.8	9	9.9
σ (%)	10	11	10	12
ZFC mode				
M_r/M_s	0.5	0.5	0.43	0.18
H_c (mT)	160	185	145	382
FC mode				
M_r/M_s		0.5		0.33
H_c (mT)		185		895

3.2.2. Co_{hcp} (3.7 nm)@CoO (3.1 nm) core shell nanoparticles

In the following analysis, we will shift our attention to the highly crystallized system comprising Co_{hcp} (3,7 nm)@CoO (3.1 nm) NPs to compare its magnetic properties to those of the poorly crystallized ones, specifically Co_{fcc}@CoO NPs. For the starting highly crystallized Co hcp NPs (*ZFC mode*) (Fig. 5A), the saturation was reached at around 3T, the coercive field was found at 145 mT and the M_r/M_s was equal to 0.43 of the metal NPs (Table 1). These observed values are in agreement with the expected magnetic properties of cobalt hcp metallic nanoparticles, as previously reported (32).

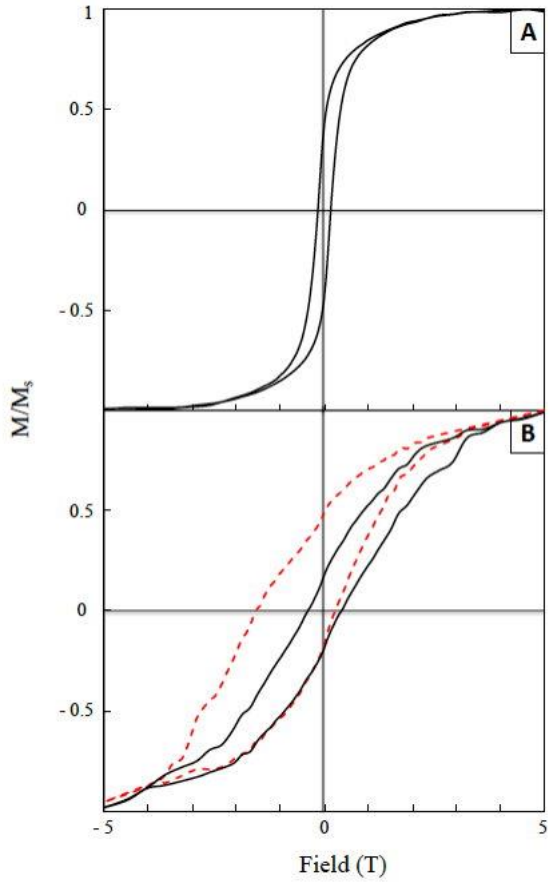

Figure 5. Hysteresis curves taken at 3K of (A) Co hcp nanoparticles (solid line) and (B) Co_{hcp}@CoO nanoparticles in ZFC mode (solid line) and FC mode (dashed line).

Subsequent to the oxidation that transformed the nanoparticles into Co_{hcp}@CoO, the hysteresis loop (*ZFC mode*), showed an increase of H_c from 145 to 382 mT. This behavior aligned with the expected feature of an interface between FM and AFM regions in the case of poorly crystallized Co fcc NPs.

When this magnetization curve with a field of 5T was applied during the cooling from 300 to 3 K (*FC mode*), a large shift of the hysteresis loop along the magnetic field axis, with a coercive field of 895 mT (Fig. 5B), was observed while the hysteresis loop in ZFC *mode* was, as expected, symmetrical. Notably, in the highly crystallized system, the AFM (CoO) was highly crystallized with a large magnetocrystalline anisotropy. This favor, through its coupling with FM, an exchange bias effect, H_{EB} = 655 mT. In this case, the FC cooling induced the AFM ordering of the spins in CoO. Thereafter, the AFM exerted a pinning action on the magnetization of the FM which gave rise to a significant loop shift.

As reported by Nogues et al. [39], various factors can influence the efficiency of exchange interactions and therefore the H_{EB} value. In the case of nanoparticles, for a ferromagnetic core

(FM) covered by an antiferromagnetic layer (AFM), we need to take into account the roughness of the interface, the crystalline state (amorphous or not) of the surface of the metal core on which oxide layer grows, the homogeneity of the interface or the presence of impurities.

The analysis of the correlation between H_{EB} behavior and the thickness of the oxide layer presents a complex challenge. However, empirical evidence generally indicates a decreasing trend of H_{EB} with increasing thickness of the oxide layer. Note here that the surface oxide layer thickness of Co fcc (2.2 nm) is slightly less than that of Co hcp (3.1 nm). This may work against exchange for Co fcc/CoO.

But the main effect is due to the different crystallinity of the Co (metal)/CoO interface. Indeed, Nogues et al. [39] showed that in this case, due to the inhomogeneity of the interface, the exchange coupling decreases in the case of polycrystals (Co fcc case) compared to single crystals (Co hcp case). Similarly, the roughness of the interface and, above all, its amorphous nature reduce the value of H_{EB}, since the latter strongly depends on the spin structure at the interface and therefore on the alignment of the spins between the ferromagnetic core and the antiferromagnetic shell.

A ligand effect cannot be ruled out, but it is difficult to quantify. Nogues et al. [39] also reported that the presence of impurities at the interface (C, H or H_2O) tends to decrease the H_{EB} value. In the case of an oxide layer growing on passivated NPs, the presence of such impurities is to be expected, especially as the ligand/metal interaction is strong, which again works against Co fcc since, as mentioned above, the carboxylate-Co interaction is stronger than the amine-Co interaction.

It is therefore the effect of the nanocrystallinity of the cobalt NPs, and then of the Co/CoO interface, which are primarily responsible for the effects observed here.

This result clearly evidences the importance of the crystallinity of Co@CoO NPs, in the metallic core, the oxide shell as well as the vicinity of the interface Co/CoO, on the exchange bias effect.

To the best of our knowledge, the H_{EB} value found here for the Co(hcp)@CoO NPs, i.e. 655 mT, is higher than the ones reported in the literature for such core/shell NPs with an hcp cobalt core (Table 2). This behavior could be attributed to (1) the high hcp crystallinity of the core/shell NPs as well as (2) their optimal geometry. Undeniably, it is shown that the exchange bias in such NPs reaches a maximum when the core and shell dimensions are similar [16], (Table 2), as in our case.

Table 2
Structural parameters and exchange bias field of Cohcp@CoO nanoparticles reported in the literature.

Co_{hcp}/CoO NPs	Co core size (nm)	CoO shell thickness (nm)	Co/CoO size (nm)	Field cooled (T)	Exchange bias field (mT)	Reference
	3.7	3.1	9.9	5	655	This study
	2.5	2.5	7.5	5	434	[11]
	10.6	1.9	14.4	0.5	48	[15]
	13.3	3	19.3	1	80	[19]
	9	3.4	15.8	5	257	[20]
	13	8	29	5	60	[23]
	13 × 130	1.2	15.4 × 132.4	5	100	[17]

Conclusion

In this paper, we have shown our findings on the partial solution-oxidation of Co fcc polycrystals and Co hcp single crystals which led to the formation of CoO fcc shell, poorly and highly crystallized respectively. Through a meticulous and accurate comparative magnetic investigation, we have highlighted the significant role played by the crystalline structure, particularly in the vicinity of the Co/CoO interface, in the resulting core/shell NPs. Notably, the observed exchange bias effect is exclusively witnessed in the highly-crystallized Co_{hcp}/CoO core shell NPs. The remarkably high value of H_{EB} found can be attributed to both the superior crystallinity of the NPs as well as the optimal ratio of the core diameter to the shell thickness in the NPs.

We would like to express our sincere gratitude to Dr. Vincent Russier of ICMPE, Université Paris-Est Créteil, for his invaluable contributions and insightful discussions throughout this research endeavor. Appreciation is also due to Dr David Hrabovsky from the MPBT (physical properties – low temperature) platform of Sorbonne University for fruitful discussions.

References:

1- W.H. Meiklejohn, C.P. Bean, New magnetic anisotropy, Phys. Rev. 102 (1956) 1413–1414.

2- J. Nogués, J. Sort, V. Langlais, V. Skumryev, S. Suriñach, J.S. Muñoz, M.D. Baró, Exchange bias in nanostructures, Physic Reports. 422 (2005) 65–117.

3- W.Zhang, K.M. Krishnan, Epitaxial exchange-bias systems: From fundamentals to future spin-orbitronics, Mater. Sci. Eng. 105 (2016) 1–20.

4- B. Dieny, V.S. Speriosu, S.S.P. Parkin, B.A. Gurney, D.R. Wilhoit, D. Mauri, Giant magnetoresistive in soft ferromagnetic multilayers, Phys. Rev. B 43 (1991) 1297–300.

5- E. Lottini, A. López-Ortega, G. Bertoni, S. Turner, M. Meledina, G. Van Tendeloo, C. de Julián Fernández, C. Sangregorio, Strongly exchange coupled core/shell nanoparticles with high magnetic anisotropy a novel strategy towards RE-free permanent magnets, Chem. Mater. 28 (2016) 4214–4222.

6- G.C Gazzadi, A. Borghi, A. di Bona, S. Valeri, Epitaxial growth of CoO on the (001) surface of bct cobalt, Surface Science. 1998, 402–404, 632–635.

7- A. K. Suszka, O. Idigoras, E. Nikulina, A. Chuvilin, A. Berger, Crystallography-driven positive exchange bias in Co/CoO bilayers, Phys. Rev. Lett. 109 (2012) 177205-5.

8- R. López Antón, J.A. González.; J.P. Andrés, P.S. Normile, J. Canales-Vázquez, P. Muñiz, J.M. Riveiro, J.A. De Toro, Exchange bias optimization by controlled oxidation of cobalt nanoparticle films prepared by sputter gas aggregation, Nanomaterials. 7 (2017) 61-70.

9- J.G. Ovejero, V. Godinho, B. Lacroix, M.A. García, A. Hernando, A. Fernández, Exchange bias and two steps magnetization reversal in porous Co/CoO layer, Materials and Design. 171 (2019) 107691-107700.

10- A. Sharma, J. Tripathi, S. Tripathi, Y. Kumar, K.C. Ugochukwu, D. Kumar, M. Gupta, R.J. Chaudhary, Exchange bias in Co/CoO thin films deposited onto self-assembled nanosphere arrays, J. Magn. Magn. Mater. 510 (2020) 166599-166607.

11- M. Verelst, T. Ould Ely, C. Amiens, E. Snoeck, P. Lecante, A. Mosset, M. Respaud, J.M. Broto, B. Chaudret, Synthesis and characterization of CoO, Co_3O_4, and mixed Co/CoO nanoparticles, Chem. Mater. 11 (1999) 2702-2708.

12- M. Spasova, U. Wiedwald, M. Farle, T. Radetic, U. Dahmen, M. Hilgendorff, M. Giersig, Temperature dependence of exchange anisotropy in monodisperse cobalt nanoparticles with a cobalt oxide shell, J. Magn. Magn. Mater. 272–276 (2004) 1508–1509.

13- J.B. Tracy, D.N. Weiss, D.P. Dinega, M.G Bawendi, Exchange biasing and magnetic properties of partially and fully oxidized colloidal cobalt nanoparticles, Phys. Rev. B 72 (2005), 064404-1 - 064404-8.

14- J.B. Tracy, M.G. Bawendi, Defects in CoO in oxidized cobalt nanoparticles dominate exchange biasing and exhibit anomalous magnetic properties, Phys. Rev. B. 74 (2006) 184434-1 - 184434-11.
15- D. Srikala, V.N. Singh, A. Banerjee, B.R. Mehta, S. Patnaik, Control of magnetism in cobalt nanoparticles by oxygen passivation, J. Phys. Chem. C. 112 (2008) 112 13882–13885.
16- S. E. Inderhees, J.A. Borchers, K.S. Green, M. Kim, K. Sun, G.L. Strycker, M.C. Aronson, Manipulating the magnetic structure of Co core/CoO shell nanoparticles: Implications for controlling the exchange bias, Phys. Rev. Lett. 101 (2008) 117202-1 - 117202-4.
17- T. Maurer, F. Zighem, F. Ott, G. Chaboussant, G. André, Y. Soumare, J.Y. Piquemal, G. Viau, C. Gatel, Exchange bias in Co/CoO core-shell nanowires: Role of antiferromagnetic superparamagnetic fluctuations, Phys. Rev. B 80 (2009) 064427-1 - 064427-9.
18- K. Simeonidis, C. Martinez-Boubeta, O. Iglesias, A. Cabot, M. Angelakeris, S. Mourdikoudis, I. Tsiaoussis, A. Delimitis, C. Dendrinou-Samara, O. Kalogirou, Morphology influence on nanoscale magnetism of Co nanoparticles: Experimental and theoretical aspects of exchange bias, Phys. Rev. B. 84 (2011) 144430-1 - 144430-10.
19- S. Chandra, H. Khurshid, M-H. Phan, H. Srikanth, Asymmetric hysteresis loops and its dependence on magnetic anisotropy in exchange biased Co/CoO core-shell nanoparticles, Appl. Phys. Lett. 101 (2012) 232405- 1 - 232405- 5.
20- M. Feygenson, E.V. Formo, K. Freeman, N. Schieber, Z. Gai, A.J. Rondinone, Implications of room temperature oxidation on crystal structure and exchange bias effect in Co/CoO nanoparticles, J. Phys. Chem. C 119 (2015) 26219−26228.
21- S. Thomas, K. Reethu, T. Thanveer, M. T. Z. Myint, S.H. Al-Harthi, Effect of shell thickness on the exchange bias blocking temperature and coercivity in Co-CoO core-shell nanoparticles, J. Appl. Phys. 122 (2017) 063902-1 - 063902- 8.
22- B. Guo, Y. Xu, S. Zhou, Morphology dependence of low temperatures exchange bias Co/CoO core-shell nanoparticles/spheres by eco-friendly solvothermal route, AIP Advances. 8 (2018) 115115-1 - 115115-5.
23- M. Ghoshani, M. Mozaafari, P.S. Normile, J.A. De Toro, A. Al-Nabhani, Core size and interface impact on the exchange bias of cobalt/cobalt oxide nanostructures. Magnetochemistry. 7 (2021) 40-53.
24- J. Nogues, V. Skumryev, J. Sort, S. Stoyanov, G. Givord, Shell-driven magnetic stability in core-shell nanoparticles, Phys. Rev. Lett. 97 (2006) 157203-157207.

25- A.N. Dobrynin, K. Temst, P. Lievens, J. Margueritat, J. Gonzalo, C.N. Afonso, E. Piscopiello, G. Van Tendeloo, Observation of Co/CoO nanoparticles below the critical size for exchange bias, J. of Appl. Phys. 101 (2007) 113913-1- 113913-8.

26- K. Kovylina, M. Garcia del Muro, Z. Konstantinovic, M. Varela, O. Iglesias, L. Labarta, X. Batlle, Controlling exchange bias in Co–CoO_x nanoparticles by oxygen content. Nanotechnology. 20 (2009) 175702-1 - 175702-8.

27- G. Salazar-Alvarez, J. Geshev, S. Agramut-Puig, C. Navau, A. Sánchez, S. Sort, J. Nogués, Tunable high-field magnetization in strongly exchange-coupled freestanding Co/CoO core/shell coaxial nanowires, ACS Appl. Mater. Interfaces 8 (2016) 22477-83.

28- T.Blachowicz, A. Ehrmann, Exchange bias in thin films—An update, Coatings. 11 (2021) 122-143.

29- M.-H. Phan, V. Kalappattil, V. Ortiz Jimenez, Y.T.H. Pham, N. W.Y.A.Y. Mudiyanselage, D. Detellem, C.-M. Hung, A.T. Chanda, T. Eggers, Exchange bias and interface-related effects in two-dimensional van der Waals magnetic heterostructures: Open questions and perspectives, J. of Alloys and Compounds. 937 (2023) 168375.

30- C. Petit, P. Lixon, M. P. Pileni, In Situ Synthesis of Silver Nanocluster in AOT Reverse Micelles, Phys. Chem. 97 (1993) 12974-12983.

31- I. Lisiecki, M.P. Pileni, Synthesis of well-defined and low size distribution cobalt nanocrystals: The limited influence of reverse micelles, Langmuir. 19 (2003) 9486-9489.

32- (a) L. Meziane, C. Salzemann, C. Aubert, H. Gérard, C. Petit, M. Petit, Hcp cobalt nanocrystals with high magnetic anisotropy prepared by easy one-pot synthesis, Nanoscale. 8 (2016) 18640–18645. (b) A. Sodreau A. Vivien A. Moisset, C. Salzemann C. Petit C., M. Petit Simpler and cleaner synthesis of variously capped cobalt nanocrystals applied in the Semihydrogenation of Alkynes, Inorg. Chem. 59 (2020) 13972−13978.

33- I. Lisiecki, C. Salzemann, D. Parker, P.A. Albouy, M.P. Pileni, Emergence of new collective properties of cobalt nanocrystals ordered in fcc supracrystals: I, Structural investigation, J. Phys. Chem. C 111 (2007) 12625-12631.

34- D. Parker, I. Lisiecki, C. Salzemann, M.P. Pileni, Emergence of new collective properties of cobalt nanocrystals ordered in fcc supracrystals: II, Magnetic investigation, J. Phys. Chem. C. 111 (2007) 12632-12638.

35- S.C. Petitto, E.M. Marsh, G.A. Carson, M. A. Langell, Cobalt oxide surface chemistry: The interaction of CoO (100), Co_3O_4 (110) and Co_3O_4 (111) with oxygen and water, J. Mol. Catal. A Chem. 281 (2008) 49–58.

36- A. Cazacu, C. Larosa, P. Beaunier, G. Laurent, P. Nanni, L. Mitoseriu, I. Lisiecki, Self-organization and/or nanocrystallinity of Co nanocrystals effects on the oxidation process using high-energy electron beam, Adv. Funct. Mater. 24 (2014) 164–170.
37-K. Kazḿierczak, D. Yi, A. Jaud, P.-F. Fazzini, M. Estrader, G. Viau, P. Decorse, J.-Y. Piquemal, C. Michel, M. Besson, K. Soulantica, N. Perret, Influence of capping ligands on the catalytic performances of cobalt nanoparticles prepared with the organometallic Route, J. Phys. Chem. C 125 (2021) 7711−7720.
38- S. Mourdikoudis, M. Menelaou, N. Fiuza-Maneiro, G. Zheng, S. Wei, J. Pérez-Juste, L. Polavarapu, Z. Sofer, Oleic acid/oleylamine ligand pair: a versatile combination in the synthesis of colloidal nanoparticles, Nanoscale Horiz. 7 (2022) 941-1015.
39- J. Nogues, I. K. Schuller, Exchange bias, J. Magn. Magn. Mater 192 (1999) 203—232.